Dyes and Pigments 92 (2011) 610–618

Contents lists available at ScienceDirect

Dyes and Pigments

journal homepage: www.elsevier.com/locate/dyepig

Synthesis, characterization, electrochemistry and spectroelectrochemistry of novel soluble porphyrazines bearing unsaturated functional groups

Serap Tuncer [a], Atıf Koca [b], Ahmet Gül [c,*], Ulvi Avcıata [a]

[a] Department of Chemistry, Yıldız Technical University, Davutpasa 34210, Istanbul, Turkey
[b] Chemical Engineering Department, Engineering Faculty, Marmara university, Kadıköy, 34722, Istanbul, Turkey
[c] Department of Chemistry, Technical University of Istanbul, Maslak 34469, Istanbul, Turkey

ARTICLE INFO

Article history:
Received 2 May 2011
Received in revised form
17 May 2011
Accepted 27 May 2011
Available online 16 June 2011

Keywords:
Porphyrazines
Magnesium
Cobalt
Spectroelectrochemistry
Cyclic Voltammetry
Chromaticity diagram

ABSTRACT

Metalloporphyrazines with a 2-methyl-2-pentenyl group fused to each pyrrole unit were synthesized starting with the corresponding unsaturated dicarbonitrile derivative. The new compounds were characterized by elemental analysis together with FTIR, ^{1}H-NMR, and UV–Vis spectroscopy and via voltammetric and spectrochemical methods. Electrochemical and spectroelectrochemical measurements demonstrate that while metal-free and magnesium porphyrazines gave common porphyrazine (Pz) ring-based electron-transfer reactions, incorporating redox active metal center, Co^{II}, into the porphyrazine core extended the redox activity of the ring system with reversible metal-based reduction and oxidation couples of the metal center in addition to the common Pz ring-based electron transfer processes. The unsaturated functional groups of the porphyrazines did not alter the common electrochemical behavior of the complexes. An *in situ* electrocolorimetric method, based on the 1931 CIE (Commission Internationale de l'Eclairage) system of colorimetry, was applied to investigate the color of the electrogenerated anionic and cationic forms of the complexes for possible electrochromatic applications.

1. Introduction

Metalloporphyrazines (MPzs) with an extended delocalized 18 π-electron conjugated macrocyclic system, which exhibit high thermal stability, chemical reactivity, and unique electrochemical performance, are usually used as photo- and electrocatalyst [1,2]. A range of different substituents provides porphyrazine ligands with interesting new features such as greatly enhanced organic solubility compared to their phthalocyanine counterparts. Peripheral heteroatom functionalization of the porphyrazine macrocycle results in significant modulation of their physical and electronic properties [3,4]. Barrett, Hoffman and co-workers have published extensively on the synthesis of porphyrazines bearing thiols, amines or alcohols as ring substituents, with the conversion of the resulting polydentate ligands to a variety of coordination complexes [3,4]. Our research group has reported the synthesis of porphyrazines bearing tertiary-quaternized aminoethyl and tosylamine, ferrocene, crown ether and dithiaheterocycles as ring substituents [5–12]. Studies on the porphyrazines in the literature indicate that design of novel substituted tetrapyrrole derivatives closely follows the requirements of their intended applications. Execution of minor changes on the nature and position of side groups or using different metal ions in the inner core can be considered as practical methods of tuning the properties of these materials. Intensive research interest in peripherally functionalized porphyrazines during the last decade has shown that these tetrapyrrole derivatives should be considered as alternatives to the phthalocyanines that have found extensive applications in material science and the photodynamic therapy of tumors as well as pigments and dyes, liquid crystal materials, electrochemical metal sensors, gas sensors, as well as good electrochemical and optical properties and catalytic behavior [13–16]. In the present work, we have synthesized metalloporphyrazines with 2-methyl-2-pentenyl group fused to each pyrrole in order to investigate their voltammetric, *in situ* spectroelectrochemical, and *in situ* electrocolorimetric responses to open a way to their possible technological applications. The electrochemical properties of inactive metal-centered metalloporphyrazine derivatives are compared with the electrochemical properties of redox active metal-metalloporphyrazines. In addition, the effects of 2-methyl-2-pentenyl groups fused to each pyrrole of the porphyrazines on the electrochemical properties of the system have been investigated in detail.

* Corresponding author. Tel.: +90212 2856827; fax: +90212 2856386.
E-mail address: ahmetg@itu.edu.tr (A. Gül).

0143-7208/$ – see front matter © 2011 Elsevier Ltd. All rights reserved.
doi:10.1016/j.dyepig.2011.05.023

2. Experimental

2.1. Instruments and chemicals

Dichloromethane (DCM), Chloroform ($CHCl_3$), ethanol (C_2H_5OH), *n*-butanol, ethyl acetate, methanol, trifluoroacetic acid (CF_3COOH), *n*-hexane, tetrahydrofuran (THF) were purchased from Merck (Germany). 5-Bromo-2-methyl-2-pentene and cobalt(II) acetate was purchased from Alfa Aesar (Germany). *Tetra*butylammonium tetrafluoroborate ($TBABF_4$) and tetrabutylammonium pechlorate (TBAP) were purchased from Sigma-Aldrich (Germany). All reagents and solvents were of reagent grade quality and were obtained from commercial suppliers.

IR spectra were recorded on a Mattson 1000 FTIR spectrophotometer using KBr pellets, electronics absorption spectra on an Agilent 8453 UV–vis spectrophotometer. Elemental analyses were carried out Slashea 1112 Serie Thermo. ^{1}H NMR spectra were recorded on a Bruker 250 MHz spectrometer using $SiMe_4$ as a reference. The homogeneity of the products was tested at each step by TLC (SiO_2).

2.2. Electrochemical studies

Electrochemical and spectroelectrochemical measurements were carried out with a Gamry Reference 600 potentiostat/galvanostat utilizing a three-electrode configuration at 25 °C. For the cyclic voltammetry (CV), and square wave voltammetry (SWV) measurements, the working electrode was a platinum disc with a surface area of 0.071 cm^2. The surface of the working electrode was polished with a diamond suspension before each run. A platinum wire served as the counter electrode. A saturated calomel electrode (SCE) was employed as the reference electrode and separated from the bulk of the solution by a double bridge. Ferrocene was used as an internal reference. Tetrabutylammonium perchlorate (TBAP) in dichloromethane (DCM) was employed as the supporting electrolyte at a concentration of 0.10 mol dm^{-3}. High purity N_2 was used to remove dissolved O_2 at least 15 min prior to each run and to maintain a nitrogen blanket during the measurements. IR compensation (A way to compensate for the voltage drop across resistance of the electrochemical system) was applied to the CV and SWV scans to minimize the potential control error. UV/Vis absorption spectra and chromaticity diagrams were measured by an OceanOptics QE65000 diode array spectrophotometer. *In situ* spectroelectrochemical measurements were carried out utilizing a three-electrode configuration of thin-layer quartz spectroelectrochemical cell at 25 °C. The working electrode was platinum tulle. A platinum wire counter electrode and an SCE reference electrode were used, separated from the bulk by a double bridge.

In situ electrocolorimetric measurements, under potentiostatic control, were obtained using an OceanOptics QE65000 diode array spectrophotometer in color measurement mode by utilizing a three-electrode configuration of thin-layer quartz spectroelectrochemical cell. The standard illuminant A with 2° observer at constant temperature in a light booth designed to exclude external light was used. Prior to each set of measurements, background color coordinates (*x*, *y*, and *z* values) were taken at open-circuit, using the electrolyte solution without the MPz under study. During the measurements, readings were taken as a function of time under kinetic control.

2.3. Synthesis

2.3.1. Synthesis of 1,2-bis(2-methyl-2-pentenyl)maleonitrile (1)

0.500 g (3.07 mmol) 5-Bromo-2-methyl-2-pentene and 0.286 g (1.54 mmol) dithiomaleonitrile disodium salt were heated under reflux with stirring in 5.0 cm^3 absolute ethanol at ~50 °C for 24 h. The solvent was evaporated and a little amount of $CHCl_3$ was added to remove unreacted maleonitrile salt from the oily-yellow ligand at 4 °C. Yield: 0.30 g, 60%. Anal. Calc. for $C_{16}H_{22}N_2S_2$: C, 62.74; H, 7.19; N, 9.14; S, 20.93. Found: C, 62.70; H, 7.15; N, 9.10; S, 20.89%. FTIR ν_{max}/cm^{-1}:2970, 2928, 2855 (aliphatics), 2209 (−C≡N), 1672, 1498, 1171, 840. ^{1}H NMR (d-chloroform, 250 MHz):1.63 (s, 6H, $-CH_3$), 1.71 (s, 6H, $-CH_3$), 2.40 (q, J = 7.42 Hz, 4H, $-CH_2-$), 3.10 (t, J = 7.42 Hz, 4H, $-SCH_2-$), 5.12 (m, 2H, =CH) ppm.

2.3.2. Synthesis of octakis-2,3–7,8–12,13–17,18-(2-methyl-2-pentenyl)porphyrazinato magnesium(II) (2)

0.033 g (1.34 mmol) Mg powder was dissolved by refluxing overnight in 10.0 cm^3 *n*-BuOH with addition of a few I_2 crystals. To the magnesium butoxide suspension formed, 0.30 g (1.34 mmol) **1** was added and after refluxing for 10 h under N_2 a dark blue suspension was obtained at 130–140 °C. The solvent was evaporated from the oily-dark blue product. Finally the product **2** was purified by column chromatography with ethyl acetate (EtOAc)/*n*-hexane (1:3) eluent. Compound **2** was fairly soluble in $CHCl_3$ and THF. Yield: 0.21 g (%70) Anal. Calc. for $C_{64}H_{88}N_8S_8$ Mg: C: 61.51; H: 7.04; N: 8.96; S: 20.52. Found: C: 61.48; H: 7.01; N: 8.93; S: 21.49%. FTIR ν_{max}/cm^{-1} :2963, 2912, 2850 (aliphatics), 1435, 1016, 884, 792, 759. ^{1}H NMR (d-chloroform, 250 MHz): 1.61 (br s, 24H, $-CH_3$), 1.71 (br s, 24H, $-CH_3$), 2.45 (br s, 16H, $-CH_2-$), 4.16 (br s, 16H, $-SCH_2-$), 5.27(m, 8H, =CH) ppm. UV–Vis λ_{max} (nm) (log ε) in $CHCl_3$: 677 (4.43), 376 (4.37).

2.3.3. Synthesis of octakis-2,3–7,8–12,13–17,18-(2-methyl-2-pentenyl)porphyrazine (II) (3)

0.20 g (0.160 mmol) **2** was demetallised by treatment with 4 cm^3 CF_3COOH at room temperature for 2 h and then the mixture was added dropwise into the ice water. The medium was neutralized with 25% NH_3 solution. It was then filtered, washed with water, and the oily-violet compound 3 was then extracted into $CHCl_3$. The solvent was evaporated and the compound **3** was purified by column chromatography with EtOAc/*n*-Hexane (1:3) eluent and then it **3** was dried on anhydrous Na_2SO_4. Compound **3** was fairly soluble in $CHCl_3$ and THF. Yield: 115 mg, 58%. Anal. Calc. for $C_{64}H_{90}N_8S_8$: C: 62.63; H: 7.33; N: 9.12; S: 20.90. Found: C: 62.59; H: 7.30; N: 9.11; S: 20.91%. FTIR ν_{max}/cm^{-1}:3279 (−NH groups in core), 2960, 2923, 2854 (aliphatics), 1462, 1137, 741. ^{1}H NMR (d-chloroform, 250 MHz): 1.59 (br s, 24H, $-CH_3$), 1.65(br s, 24H, $-CH_3$), 2.54 (br s, 16H, $-CH_2-$), 4.19 (br s, 16H, $-SCH_2-$), 5.14 (m, 8H, =CH) ppm. UV–Vis λ_{max} (nm) (log ε) in $CHCl_3$: 712 (4.53), 638 (4.30), 355 (2.47).

2.3.4. Synthesis of octakis-2,3–7,8–12,13–17,18-(2-methyl-2-pentenyl)porphyrazinato cobalt (II) (4)

0.177 g (0.144 mmol) (**3**) in 5 cm^3 THF was refluxed with 0.352 g (1.44 mmol) anhydrous $Co(CH_3COO)_2$ in 5.0 cm^3 EtOH for 24 h. After filtration, the filtrate was evaporated to dryness. The sticky product formed was washed with hot water and dried on anhydrous Na_2SO_4. The dark blue product **4** was purified by column chromatography with EtOAc/*n*-hexane (1:3) eluent. This compound was soluble in $CHCl_3$ and THF. Yield: 0.080 g, 45.2%. Anal. Calc. for $C_{64}H_{88}N_8S_8Co$: C: 59.86; H: 6.85; N: 8.72; S: 19.97. Found: C: 59.84; H: 6.82; N: 8.69; S: 19.95%. FTIR ν_{max}/cm^{-1} :2967, 2930, 2870 (aliphatics), 1435, 1360, 1219, 1040, 909, 802, 753. UV–Vis λ_{max} (nm) (log ε) in $CHCl_3$: 647 (4.23), 341 (4.25).

3. Results and discussion

3.1. Synthesis and characterization

All synthetic procedures leading to porphyrazines were started with unsaturated dithiomaleonitrile disodium salt with heterocyclic

units directly fused to these functional groups. 1,2-dinitrile was firstly oxidized to an intermediate with addition of 5-bromo-2-methyl-2-pentene to obtain 1,2-bis(2-methyl-2-pentenyl)maleonitrile (**1**) in EtOH. The cyclotetramerization process of **1**, in the presence of magnesium butoxide gave the magnesium porphyrazine derivate (MgPz), **2**, in *n*-butanol (Fig. 1). Treatment of **2** with trifluoroacetic acid, at room temperature afforded the metal-free derivative, **3**. Apparent differences between metal- and metal-free derivatives are the change in color from dark blue to violet and lowering of solubility. Conversion of the metal-free porphyrazine into the cobalt porphyrazine complex was performed by treating with $Co(CH_3COO)_2$ in EtOH-THF solvent [5–8,17].

The structures of the novel compounds were confirmed by elemental analysis together with FTIR, ^{1}H NMR, and UV–Vis spectroscopic techniques. FTIR spectra of 1,2-bis(2-methyl-2-pentenyl) maleonitrile (**1**) clearly indicated the presence of –C≡N groups at 2209 cm^{-1} as intense absorption. The IR spectra of porphyrazines confirmed the formation of the macrocycles. Cyclomerization of the dinitriles in 1,2-bis(2-methyl-2-pentenyl)maleonitrile to form MgPz **(2)** was confirmed by the disappearance of the –C≡N at 2209 cm^{-1}. NH groups in the center of the metal-free derivative, **3**, gave an absorption peak at 3279 cm^{-1} [7,8]. C–H stretching of aliphatic groups, CH_3, CH_2 and CH, in all compounds occurred on 2960–2850 cm^{-1} regions. The most revealing data for a tetrapyrrole system are given by their UV–vis spectra in solution. The metal-free derivatives have D_{2h} symmetry, their $\pi_1 \rightarrow \pi_{1,2}^*$ ($au \rightarrow b_{2g}$, b_{3g}) and $\pi_1 \rightarrow \pi_{1,2}^*$ ($b_{1u} \rightarrow b_{2g}$, b_{3g}) electronic transitions correspond to the Q and B-bands seen as two peaks, relatively. Metal containing porphyrazines have D_{4h} symmetry, their π_1^* and π_2^* orbitals are degenerate. Thus, the π_1 and $\pi_2 \rightarrow \pi_{1,2}^*$ electronic transition and the Q-band appears as one peak in the visible spectrum [18]. While MgPz exhibited an intense Q-band at 677 nm with a relatively sharp absorption peak and almost no shoulder on the higher energy side, which would correspond to aggregated species, the metal-free derivative gave a split Q-band at 638 and 712 nm. The presence of Co(II) instead of Mg(II) in the core of the porphyrazine ring shifted the Q-band from 677 to 647 nm.

The ^{1}H NMR spectra are also consistent with proposed structures. In compounds **1, 2** and **3,** two types of $-CH_3$ protons appear at higher field as a sharp singlet at 1.59, 1.71 ppm $-CH_2$ protons appear at 2.40–2.54 ppm ranges as a quartet. All compounds give a $-SCH_2$ a triplet at 3.10–4.19 ppm ranges, while =CH protons are a multiplet at the lower field at 5.12–5.27 ppm range. Due to the lower solubility of porphyrazine products, their ^{1}H NMR spectra are rather broad for the compound **2** and **3**.

3.2. Electrochemical measurements

The CV and SWV measurements of the complexes were studied in TBAP/DCM electrolyte system on a platinum electrode vs. SCE reference electrode. Table 1 lists the electrochemical parameters, which included half-wave peak potentials ($E_{1/2}$), forward to reverse peak p (ΔE_p), anodic to cathodic peak current ratios (I_{pa}/I_{pc}), and difference between the first oxidation and reduction processes ($\Delta E_{1/2}$). Peak to peak separations, $E_{1/2}$ and $\Delta E_{1/2}$ values are in agreement with the reported data for redox processes in metalloporphyrazines complexes in the literature [1,9,11,19–28]. The number of electrons transferred is unity for all redox processes. In these type complexes, multi-electron metal and/or ring-based processes occurring in one step are not common.

Metal-free porphyrazine (H_2Pz, **3**) and (MgPz, **2**) exhibited very similar voltammetric responses with small potential shifts due to the different effective nuclear charge of the Pz ring core. Within the electrochemical window of TBAP/DCM, these compounds underwent an oxidation and three reduction couples during CV and SWV measurements. Fig. 2 illustrates the CV and SWV of **3**. The compound **3** underwent a one-electron oxidation at 1.19 V, and three one-electron reduction couples at −0.45, −0.76 and −1.22 V vs. SCE at 0.100 V s^{-1} scan rate. For the first reduction couples, I_{pa}/I_{pc} values are close to unity at all scan rates demonstrating chemical reversibility of the process. However, forward to reverse peak potential separations (ΔE_p) of the couple were very large, changing from 130 to 300 mV with the scan rates from 0.010 to 0.500 mV s^{-1} (ΔE_p values were changed from 60 to 110 mV for ferrocene),

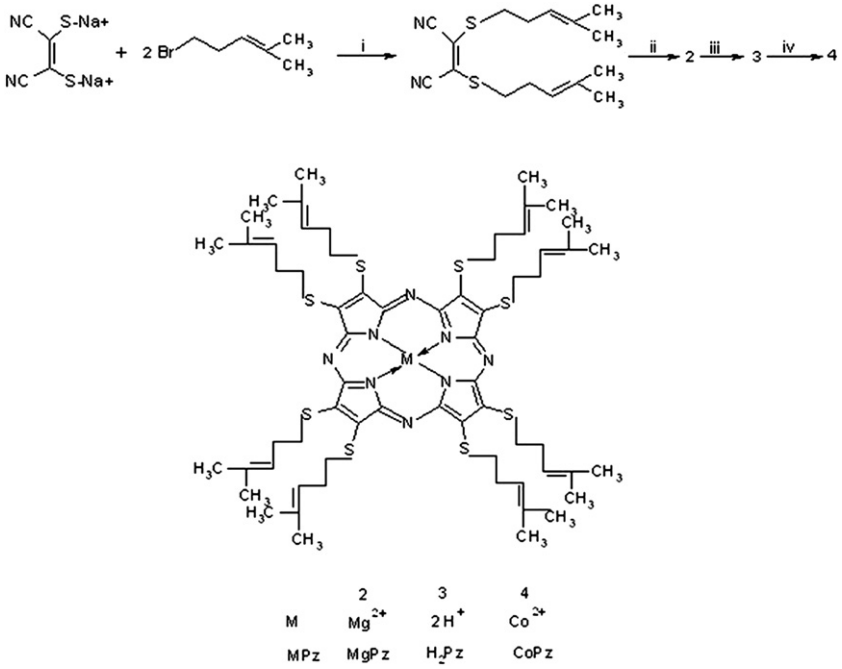

Fig. 1. Synthesis scheme for the new products 1–4. Discarbonitrile 1 and the porphyrazines derived from it.(i) EtOH, 50 °C, 24 h; (ii) $Mg(BuO)_2$, BuOH, 120 °C, 24 h; (iii) CF_3COOH, r. t.; (iv) $Co(OAc)_2$, THF, EtOH in the case of 4.

Table 1
Voltammetric data of the complexes with the related metallophthalocyanines for comparison.

Complex		Ring Oxidations		M^{III}/M^{II}	M^{II}/M^{I}	Ring Reductions			$^{d}\Delta E_{1/2}$	Ref
H2Pz (in DCM)	$^{a}E_{1/2}$ vs. SCE	–	1.19	–	–	−0.45	−0.76	−1.24	1.64	Tw
	$^{b}\Delta E_p$ (mV) vs. SCE	–	–	–	–	150	100	117		
	$^{c}I_{pa}/I_{pc}$	–	–	–	–	0.92	0.45	0.60		
MgPz (in DCM)	$^{a}E_{1/2}$ vs. SCE	1.47	0.95	–	–	−0.70	−1.07	−1.32	1.65	Tw
	$^{b}\Delta E_p$ (mV)	–	70	–	–	60	70	100		
	$^{c}I_{pa}/I_{pc}$	–	0.95	–	–	1.00	0.80	0.75		
CoPz (in DCM)	$^{a}E_{1/2}$ vs. SCE	–	–	1.40	−0.20	−1.15	–	–	1.60	Tw
	$^{b}\Delta E_p$ (mV)	–	–	–	80	97	–	–		
	$^{c}I_{pa}/I_{pc}$	–	–	–	0.98	0.94	–	–		
CoPz (in DMSO)	$^{a}E_{1/2}$ vs. SCE	–	0.77	0.34	−0.38	−1.20	–	–	1.11	Tw
	$^{b}\Delta E_p$ (mV)	–	120	100	85	62	–	–		
	$^{c}I_{pa}/I_{pc}$	–	0.47	0.35	1.00	0.95	–	–		
^{f}PbPz	$E_{1/2}$ (in DCM)	–	0.86	–	–	−0.83	−1.24	–	–	25
$^{g}H_2Pz$	$^{f}E_{1/2}$ (in DCM)	–	1.41	–	–	−0.28	−0.65	−1.56	–	10
^{g}MgPz	$E_{1/2}$ (in DCM)	–	1.15	–	–	−0.52	−0.87	−1.16	–	10
^{g}CoPz	$E_{1/2}$ (in DCM)	–	–	1.42	−0.28	−0.62	−1.60	–	–	10
$^{h}H_2Pz$	$E_{1/2}$ (in DCM)	1.09	0.90	–	–	−0.21	−0.50	−0.91	–	11
^{i}CoPyPz	$E_{1/2}$ (in DCM)	–	1.11	0.66	−0.24	−0.58	−0.97	–	–	26
^{i}ZnPyPz	$E_{1/2}$ (in DCM)	1.03	0.65	–	–	−0.73	−0.94	−1.23	–	27
$^{j}H_2Pz$	$E_{1/2}$ (in DCM vs. SHE)	–	0.90	–	–	−0.63	−0.99	–	–	28

^{a}: $E_{1/2}=(E_{pa}+E_{pc})/2$ at 0.100 V s^{-1}; ^{b}: $\Delta E_p = |E_{pa} - E_{pc}|$ at 0.100 V s^{-1}; ^{c}: I_{pa}/I_{pc} for reduction, I_{pc}/I_{pa} for oxidation processes at 0.100 V s^{-1} scan rate; ^{d}: $\Delta E_{1/2} = E_{1/2}$ (first oxidation)$-E_{1/2}$ (first reduction) = HOMO–LUMO gap for metalloporphyrazines having electro-inactive metal center (metal to ring (MLCT) or ring to metal (LMCT) charge transfer transition gap for MPz having redox active metal center.); ^{e}: The process is recorded with SWV; ^{f}: Substituted with octapropyl moieties; ^{g}: Substituted with eight (1-naphthylmethylthio) moieties; ^{h}: Substituted with octakis crown ether moieties; ^{i}: Substituted with tetrakis-2,3-(5,7-diphenyl-1,4-diazepino) moieties; ^{j}: Substituted with four $[Ru(bipy)_2Cl]^+$] moieties; Tw: This work.

demonstrating electrochemical irreversibility of the electron transfer character of the couple. Deviation of SWV from symmetry in the forward and reverse SWV scans illustrates the irreversible character of the process (Fig. 2B). The peak current increased linearly with the square root of scan rate for scan rates ranging from 0.010 to 0.500 mV s^{-1}, which indicates the purely diffusion-controlled behavior of this couple [29]. For second and third redox couples, ΔE_p values were very large and I_{pa}/I_{pc} values were less than unity at all scan rates, suggesting both chemical and electrochemical irreversibility of the electron transfer processes and the existence of a chemical reaction following the electron transfer processes. Recording CV with different switching potentials did not alter the redox characters of the reduction processes.

Fig. 3 illustrates the CV and SWV of **2**. Differences between electrochemical responses of **2** and **3** are due to the redox potentials and aggregation tendencies of the complexes. When the magnesium center of **2** was exchanged with hydrogen to form **3**, the redox potentials shifted to the positive. As a result of this potential shift

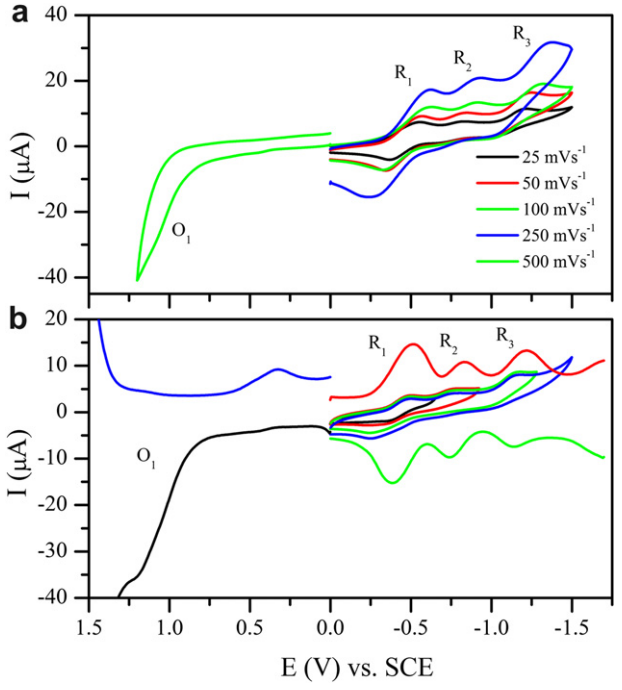

Fig. 2. A) CVs of 3 ($5.0\ 10^{-4}$ mol dm^{-3}) at various scan rates on Pt in DCM/TBAP. B) SWVs and CVs of 3 recorded with different switching at 0.100 V s^{-1} scan rate.

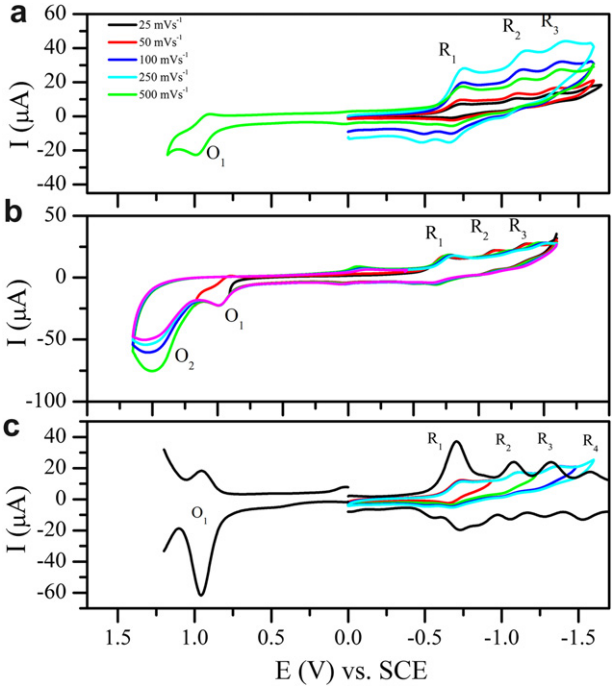

Fig. 3. A) CVs of 2 ($5.0\ 10^{-4}$ mol dm^{-3}) at various scan rates on Pt in DCM/TBAP. B) CVs of 2 recorded with different positive switching potentials at 0.100 V s^{-1} scan rate. C) SWV and CVs of 2 recorded with different negative switching potentials at 0.100 V s^{-1} scan rate on Pt in DCM/TBAP.

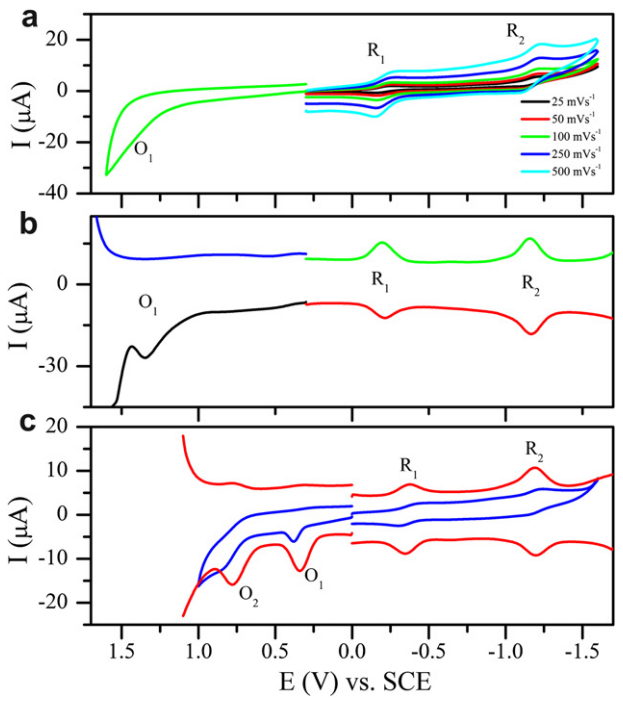

Fig. 4. A) CVs of 4 ($5.0\ 10^{-4}$ mol dm^{-3}) at various scan rates on Pt in DCM/TBAP. B) SWVs of 4 in DCM/TBAP. C) CV and SWV of 4 at 0.100 V s^{-1} scan rate on Pt in DMSO/TBAP.

the second oxidation process of **2** was recorded at 1.47 V. Recording CV with different switching potentials changed the redox character of the oxidation and reduction processes of **2** (Fig. 3B and C). During the anodic potential scan, when the potential was switched before the second oxidation reaction the redox processes did not change. However when the potential was switched after the second oxidation process, an irreversible wave was observed at −0.10 V and the second and third reduction processes disappeared during the continuous potential scans. Moreover the first oxidation process became irreversible and the peak current of the second oxidation process decreased. These voltammetric data indicate that the complex might have decomposed during the second oxidation process and products of the decomposition reaction may have deposited on the working electrode. Blockage of the working electrode surface with the products of the decomposition reaction might prevent the electron transfer of the species in the bulk solution. During the cathodic potential scan, when the potential was switched just after the first reduction process, the complex gave a well-resolved reversible couple at −0.70 V. However when the potential was switched after the first reduction process, an irreversible wave was observed at −0.48 V during the reverse scan and anodic couple of the reduction processes decreases during the continuous potential scans. These voltammetric data indicate existence of a chemical reaction succeeding the first reduction process and products of the chemical reaction being oxidized at −0.48 V.

Fig. 4 shows CVs and SWV of cobalt porphyrazine (**CoPz, 4**) recorded at different scan rates and with different switching

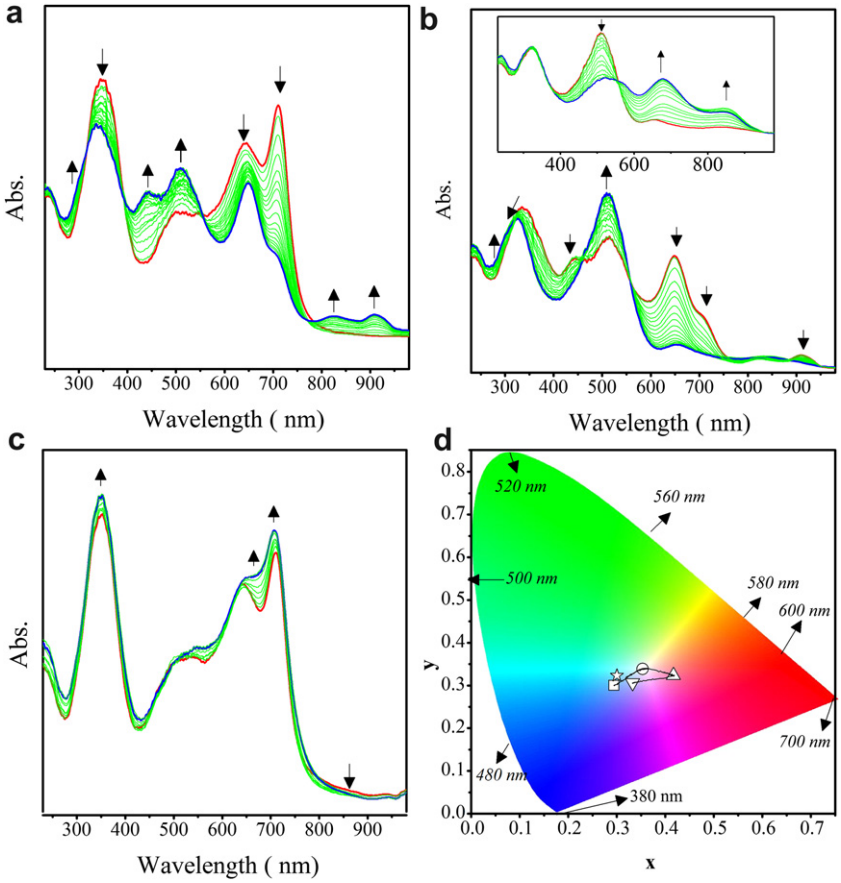

Fig. 5. *In situ* UV–vis spectral changes of 3. A) $E_{app} = -0.60$ V. B) $E_{app} = -0.85$ V (inset: $E_{app} = -1.40$ V). C) $E_{app} = 1.30$ V. D) Chromaticity diagram of 3 (each symbol represents the color of electro-generated species; □: $[H_2Pz^{-2}]$, ○: $[H_2Pz^{-3}]^{-}$, Δ:$[H_2Pz^{-4}]^{-2}$, ∇:$[H_2Pz^{-5}]^{-3}$), ☆:$[H_2Pz^{-1}]^{+1}$). (For interpretation of the references to color in this figure legend, the reader is referred to the web version of this article.)

potentials. Two well-resolved reversible and diffusion-controlled reduction couples and an oxidation wave at solvent windows of the electrolyte system are recorded [27]. Recording the CVs with different switching potentials did not change the redox characters of the redox processes. It has been reported that the complexes having redox active metal centers, e.g. Co^{II}, Fe^{II}, and Mn^{II}, may coordinate with the coordinating species present in the electrolyte system which affects the redox behaviors of the complexes [20,30]. CV and SWV of the cobalt complex were also recorded in TBAP/DMSO (coordinating solvent) electrolyte system to investigate the possible coordination of CoPz with coordinating species (Fig. 4C). In TBAP/DMSO electrolyte, oxidation couples of the complex shifted to the negative potential about 1.0 V and two oxidation processes were observed at 0.34 and 0.77 V. These data indicate that coordination of DMSO to $Co^{III}Pz^{-2}$ stabilized the cationic form of the complex and decreased the $\Delta E_{1/2}$ value of the complex. Due to the electron donating ability of DMSO, the reduction couples of the complex also shifted to the negative potentials with respect to those of the complex in DCM.

When the electrochemical responses of the porphyrazines bearing reactive 2-methyl-2-pentenyl groups were compared with complexes reported in the literature, it is clear that the reactive 2-methyl-2-pentenyl groups do not alter the electrochemical properties of the porphyrazine ring and no signal was recorded for these redox active groups. However, the electron transfer processes shifted to the positive potentials due to the electron withdrawing nature of the substituents. Besides, the presence of reactive 2-methyl-2-pentenyl groups increased the chemical reactivity of the complexes. Thus, chemical reactions followed the electron transfer reaction of the complexes were observed during the CV and SWV measurements.

3.3. Spectroelectrochemical studies

Spectroelectrochemical studies were employed to confirm the assignments in the CVs and to determine the spectra of the electrogenerated anionic and cationic forms of the complexes. To represent the *in situ* spectroelectrochemical response of the metal-free porphyrazines, spectral changes of **3** are given in Fig. 5. For the metal-free porphyrazines, the symmetry is D_{2h} and therefore there are two sharp Q-bands at 643 and 710 nm for compound **3** [2,20]. When the working electrode was polarized at −0.60 V versus SCE, $[H_2Pz^{2-}]$ was one-electron reduced to form the $[H_2Pz^{3-}]^{1-}$ anion. During the reduction of $[H_2Pz^{2-}]$ at constant potential application, the split Q-band decreased in intensity while the bands at 438, 502, 821 and 911 nm increased in intensity. Moreover, the B-band decreased with blue shift from 352 to 337 nm. During electrochemical reduction at −0.60 V, well-defined isosbestic points were observed, which demonstrated that the reduction proceeded cleanly in deoxygenated DCM to give a single, reduced species. Rollmann and Iwamoto [31] and Koca et al. [10,12] also reported similar spectroscopic changes for one-electron reduction of MPc and MPz complexes. It was mentioned that there might be a symmetry change from D_{2h} to D_{4h} because of the substitution of central hydrogens by cations from the supporting electrolyte. It was shown that the pair of excited states which usually gives rise to the Q-band doubling in the $[H_2Pz^{3-}]^{1-}$ species, was still present but the states were too close together to be resolved. During the potential

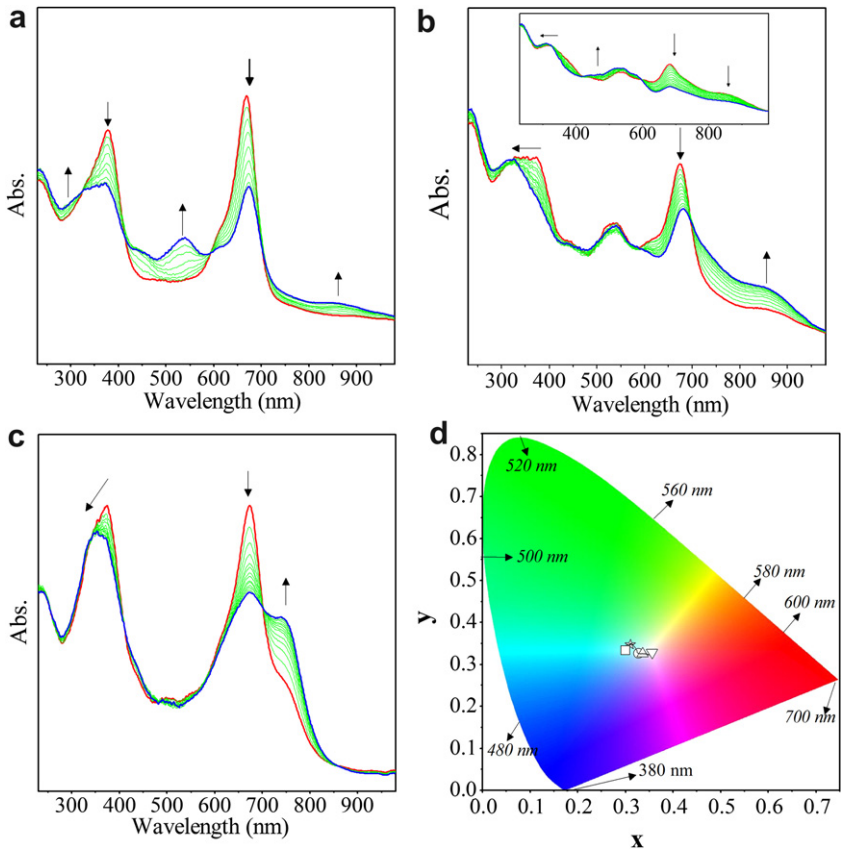

Fig. 6. *In situ* UV–vis spectral changes of 2. A) $E_{app} = -0.80$ V. B) $E_{app} = -1.20$ V (inset: $E_{app} = -1.45$ V) C) $E_{app} = 1.20$ V. D) Chromaticity diagram of 2 (each symbol represents the color of electro-generated species; □: $[MgPz^{-2}]$, ○: $[MgPz^{-3}]^{-}$, Δ:$[MgPz^{-4}]^{-2}$, ∇:$[MgPz^{-5}]^{-3}$), ☆:$[MgPz^{-1}]^{+1}$). (For interpretation of the references to color in this figure legend, the reader is referred to the web version of this article.)

application at −0.85 V versus SCE, $[H_2Pz^{3-}]^{1-}$ was one-electron reduced to form the $[H_2Pz^{4-}]^{2-}$ dianion (Fig. 5B). Spectroscopic changes show that while the B-band decreased in intensity with blue shift, the Q-bands disappeared completely. At the same time, while the band at 438 nm remained as unchanged, the band at 502 nm continued to increase. Clear isosbestic points were recorded at 318, 461, 560, 754 and 878 nm in the spectra. Inset graph of Fig. 5B represents the spectroscopic changes during the third reduction of **3**. During the oxidation of **3** at 1.30 V applied potential, considerable spectral changes were not recorded. Intensity of the Q-band and the band at 518 nm increased slightly while the intensity of the NIR region decreased (Fig. 5C).

The color changes of the complexes during the redox processes were recorded using *in situ* colorimetric measurements. Without any potential application, the solution of **3** was light blue ($x = 0.2939$ and $y = 0.3006$) (Fig. 5D). As the potential was stepped from 0 to −0.60 V, the color of the neutral $[H_2Pz^{-2}]$ started to change and yellow color ($x = 0.3534$ and $y = 0.3389$) of the monoanionic form of $[H_2Pz^{-3}]^{-1}$ was obtained at the end of the first reduction. Similarly, the color of the dianionic species, $[H_2Pz^{-4}]^{-2}$ was recorded as red ($x = 0.4169$ and $y = 0.3239$) and the trianionic species, $[H_2Pz^{-5}]^{-3}$ was recorded as light purple ($x = 0.3328$ and $y = 0.3065$). Monocationic species, $[H_2Pz^{-1}]^{+1}$ had same color with the neutral form of the compound (Fig. 5D). Measurement of the xyz coordinates allows quantification of each color of the redox species that is very important in deciding their possible electrochromic application.

Fig. 6 shows the spectral changes of **2**. During the controlled potential reductions of **2** at −0.80 V potential application, the intensity of the Q-band at 670 nm decreased without shift, while new bands were recorded at 539 and 860. At the same time, the B-band at 380 nm and n → π* transition band at 610 nm decreased in intensity (Fig. 6B). This process provides clear isosbestic points at 325, 414, 594, and 704 nm in the spectra. The color change from greenish blue ($x = 0.3001$and $y = 0.3337$) to light blue ($x = 0.3283$ and $y = 0.3263$) was observed by *in situ* colorimetric measurement during the process (Fig. 6D). These spectroscopic changes are characteristic of Pz ring reduction and assign the couple R_1 to the $[Mg^{II}Pz^{-2}]/[Mg^{II}Pz^{-3}]^{-1}$ process [10,12,27,28,32–34]. Spectroscopic changes during the controlled potential application at −1.20 and −1.45 V support the further reductions of the monoanionic species, $[Mg^{II}Pz^{-3}]^{-1}$, to $[Mg^{II}Pz^{-4}]^{-2}$ (Fig. 6B) and then to $[Mg^{II}Pz^{-5}]^{-3}$ (Fig. 6B inset). Decreasing of the Q-band intensity at 684 nm without shift and observation of new bands in the MLCT region are characteristics of the ring reduction processes, at the end of which a light orange color ($x = 0.3566$ and $y = 0.3288$) was obtained (Fig. 6D). During the oxidation of **2** (Fig. 6C), absorption of the Q-band decreased in intensity without shift, while a new band at 747 nm increased in intensity. At the same time, the-B-band decreased with blue shift from 380 nm to 360 nm. Clear isosbestic points were recorded at 337, 408, 477, and 702 nm in the spectra. These changes are typical of a ring-based oxidation and assigned to the $[Mg^{II}Pz^{-2}]/[Mg^{II}Pz^{-1}]^{+1}$ process [10,12,27,28,32–34].

Fig. 7 represents the *in situ* UV–Vis spectral changes and *in situ* recorded chromaticity diagram of **4** in TBAP/DCM during the potential application at the potentials of the redox processes. Shifting of the Q-band from 651 to 680 nm with decrease in intensity and observation of a new band at 570 nm indicate the metal

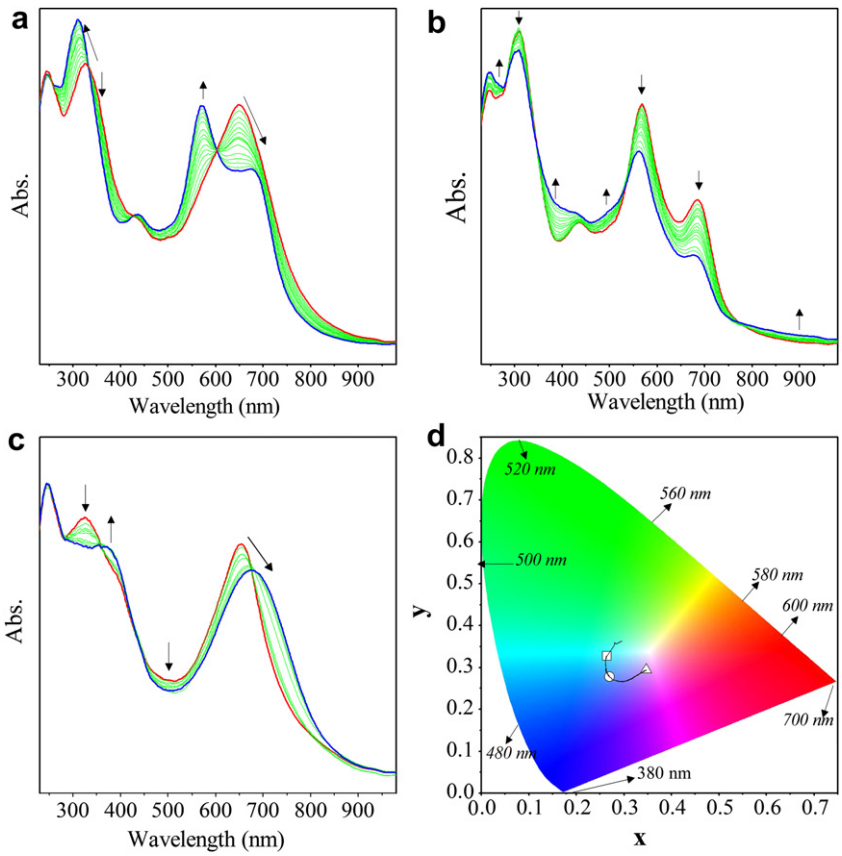

Fig. 7. *In situ* UV–vis spectral changes of 4 in DCM/TBAP. A) $E_{app} = -0.40$ V. B) $E_{app} = -1.30$ V. C) $E_{app} = 1.60$ V. D) Chromaticity diagram of 4 (each symbol represents the color of electro-generated species; □: $[Co^{II}Pz^{-2}]$, ○: $[Co^{I}Pz^{-2}]^{-}$, Δ:$[Co^{I}Pz^{-3}]^{-2}$, ☆:$[Co^{III}Pz^{-2}]^{+1}$). (For interpretation of the references to color in this figure legend, the reader is referred to the web version of this article.)

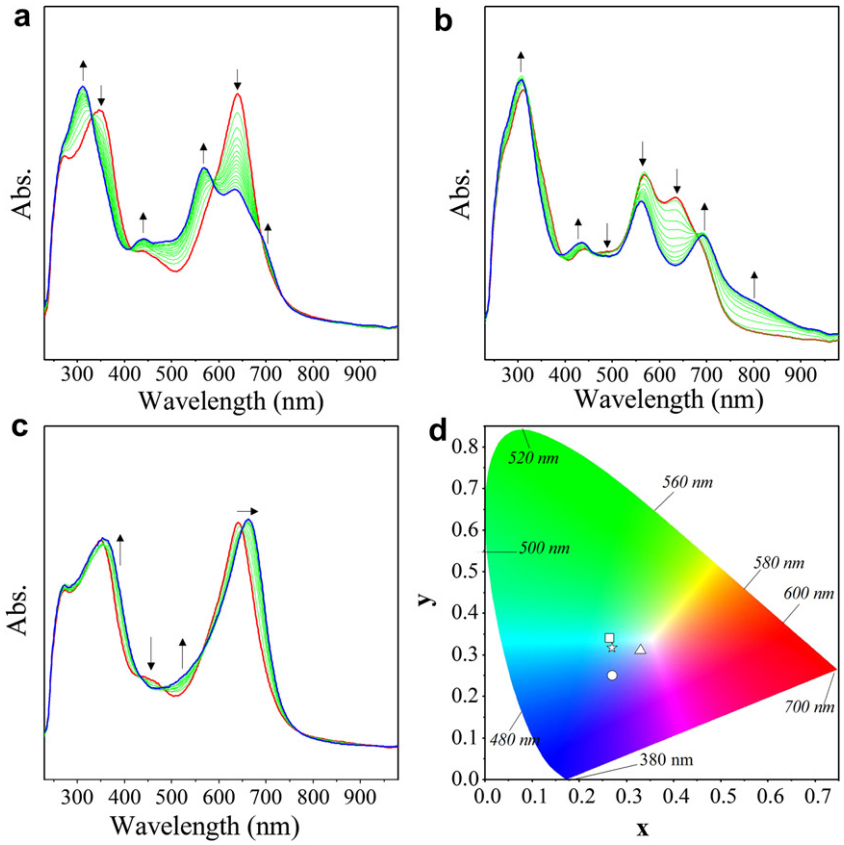

Fig. 8. *In situ* UV–vis spectral changes of 4 in DMSO/TBAP. A) $E_{app} = -0.50$ V. B) $E_{app} = -1.30$ V. C) $E_{app} = 0.50$ V. D) Chromaticity diagram of 4 (each symbol represents the color of electro-generated species; □: $[Co^{II}Pz^{-2}]$, ○: $[Co^{I}Pz^{-2}]^{-}$, Δ:$[Co^{I}Pz^{-3}]^{-2}$, ☆:$[Co^{III}Pz^{-2}]^{+1}$). (For interpretation of the references to color in this figure legend, the reader is referred to the web version of this article.)

center reduction of **4** at −0.40 V potential application (Fig. 7A). At the same time, the B-band shifted from 330 to 311 nm with increase in intensity. This process resulted in clear isosbestic points at 334, 430, and 601 nm in the spectra and a color change from greenish blue ($x = 0.264$ and $y = 0.3272$) to blue ($x = 0.2697$ and $y = 0.2777$) as shown in the chromaticity diagram (Fig. 7D). These spectroscopic data assign the first reduction couple $\mathbf{R_1}$ to $[Co^{II}Pz^{-2}]/[Co^{I}Pz^{-2}]^{1-}$. Further reduction of the $[Co^{I}Pz^{-2}]^{1-}$ at −1.30 V indicate a ligand-based redox process. Because the Q-band at 680 nm and the band at 570 nm decreased in intensity without shift while a new broad band was recorded at 495 nm. At the same time, the B-band decreased in intensity, while the band at around 390 nm increased slightly in intensity (Fig. 7B). Clear isosbestic points were recorded at 281, 345, 530, and 776 nm in the spectra. Color change from blue to purple ($x = 0.3469$ and $y = 0.2937$) was recorded (Fig. 7D). These changes assign the second reduction couple to the $[Co^{I}Pz^{-2}]^{1-}/[Co^{I}Pz^{-3}]^{2-}$. Fig. 8C represents the spectral changes during the oxidation process of the complex. During 1.60 V potential application, shifting of the Q-band from 653 to 680 nm with decrease in intensity indicates a metal-based process and is assigned to the $[Co^{II}Pz^{-2}]/[Co^{III}Pz^{-2}]^{1+}$ (Fig. 7C) [10,12,27,28,32–34]. Color change from greenish blue to green ($x = 0.2963$ and $y = 0.3619$) and isosbestic points at 360, 445, and 675 nm were recorded during the oxidation process. Fig. 8 represents the *in situ* UV–Vis spectral changes and *in situ* recorded chromaticity diagram of **4** in TBAP/DMSO during the potential application at the potentials of the redox processes. When Fig. 7 is compared with Fig. 8, it is clearly shown that complex **4** gives approximately similar spectral and chromaticity diagrams in both DCM and DMSO solvent system.

4. Conclusion

We have synthesized novel porphyrazines derivatives and the synthetic results of these materials are described. Their electrochemical and spectroelectrochemical results have been carried out. The electrochemical parameters, which included half-wave peak potentials ($E_{1/2}$), forward to reverse peak potential separation (ΔE_p), anodic to cathodic peak current ratios (I_{pa}/I_{pc}), and difference between the first oxidation and reduction processes ($\Delta E_{1/2}$) were recorded. Peak to peak separations, $E_{1/2}$ and $\Delta E_{1/2}$ values are in agreement with the reported data for redox processes in metalloporphyrazine complexes in the literature. Complexes show well-defined redox couples ascribed to metal and ring-based processes. The effects of the respective substituents on these properties were observed.

Acknowledgments

This work was supported by the Research Fund of the Yildiz Technical University and Tor Vergata University (Erasmus Program) in Rome/Italy. We are grateful to Prof. Pietro Tagliatesta for valuable helps.

References

[1] Kadish KM, Van Caemelbecke E, Royal G. In: Kadish KM, Smith KM, Guilard R, editors. The porphyrin hand book, vol. 8. Academic Press; 2000. p. 1–114.
[2] Kadish KM, Smith KM, Guilard R, editors. The porphyrin hand book, vol. 8. Academic Press; 2000. p. 114.

[3] Stuzhin PA, Ercolani C. In: Kadish KM, Smith KM, Guilard R, editors. The porphyrin handbook, vol. 15. Academic Press; 2003. p. 263.
[4] Michel SL, Baum S, Barrett AGM, Hoffman BM. In: Karlin KD, editor. Progress in inorganic chemistry, vol. 50. Wiley; 2001. p. 473.
[5] Polat M, Gül A. Synthesis of new porphyrazines with tertiary or quaternized aminoethyl substituents. Dyes Pigments 2000;45(3):195–9.
[6] Uslu RZ, Gül A. Porphyrazines with tosyamine functional groups. C R Acad Sci Paris Ser II C: Chim 2000;3(8):643–8.
[7] Akkuş H, Gül A. Octakis(ferrocene) substituted porphyrazines. Transit Metal Chem 2001;26:689–94.
[8] Sağlam Ö, Gül A. Porphyrazines with appending eight crown ethers. Polyhedron 2001;20:269–75.
[9] Erdoğmus A, Koca A, Avciata U, Gül A. Synthesis, characterization and electrochemistry of new soluble porphyrazine complexes bearing octakis 3-methylbutylthio substituents. Z Anorg Allg Chem 2008;634(14):2649–54.
[10] Koca A, Gonca E, Gül A. Voltametric and spectroelectrochemical characterization of porphyrazines: electrochemical metal sensor. J Electroanal Chem 2008;612(2):231–40.
[11] Koca A, Sağlam Ö, Gül A. Electrochemical investigation on porphyrazines with peripheral. Monats Chem 2003;1:11–21.
[12] Tuncer S, Koca A, Gül A. Avciata U.1,4-dithiaheterocycle-fused porphyrazines: synthesis, characterization, voltammetric and spectroelectrochemical properties. Dyes Pigments 2009;81:144.
[13] Luk'yanets EA. Phthalocyanines and their analogues in new fields of technology. Mol Mat 1992;1:209–16.
[14] Bekaroğlu Ö. Synthesis of phthalocyanines and related compounds. J. Porphyrins Phthalocyanine 2000;4:465–73.
[15] Sanchez M, Chap N, Cazaux JB, Meunier B. Metallophthalocyanines linked to organic copolymers as efficient oxidative supported catalysts. Eur J Inorg Chem; 2001:1775–83.
[16] Ahcar BN, Jayasree PK. Synthetic metals based on nickel(II) 2,9,16,23-tetrahalo-substituted phthalocyanine derivatives. Synth Metals 2000;114:219–24.
[17] Kobayashi N, Kadish KM, Smith KM, Guilard R. Meso-azaporphyrins and their analogues. The porphyrin handbook, vol. 2. Academic Press; 2000. pp. 301–333.
[18] Mchugh AJ, Weiss C, Gouterman M. Porphyrins, energy, oscillator strength and zeeman splitting calculations. Theo Chim Acta 1972;24:346–56.
[19] Wang C, Bryce MR, Batsanov AS, Howard JAK. Synthesis of pyrazinoporphyrazine derivatives functionalised with tetrathiafulvalene (TTF) units: X-ray crystal structures of two related ttf cyclophanes and two bis(1,3-dithiole-2-thione) intermediates. Chem Eur J 1997;10:1679–90.
[20] Liao MS, Scheiner S. Comparative study of metal-porphyrins, -porphyrazines, and -phthalocyanines. J Comput Chem 2002;23:1391–403.
[21] Miwa H, Ishii K, Kobayashi N. Electronic structures of zinc and palladium tetraazaporphyrin derivatives controlled by fused benzo rings. Chem Eur J 2004;10:4422–35.
[22] Miwa H, Makarova EA, Ishii K, Luk'yanets EA, Kobayashi N. Spectroscopy, electrochemistry, and molecular orbital calculations of metal-free tetraazaporphyrin, -chlorin, -bacteriochlorin, and -isobacteriochlorin. Chem Eur J 2002;8:1082–90.
[23] Hou R, Jin L, Yin B. Synthesis and electron donating property of novel porphyrazines containing tetrathiacrown ether-linked tetrathiafulvalene moieties. Inorg Chem Commun 2009;12:739–43.
[24] Kandaz M, Ozkaya AR, Koca A, Salih B. Water and alcohol soluble octakis metalloporphyrazines bearing sulfanyl polyetherol substituents: synthesis, spectroscopy, and electrochemistry. Dyes Pigments 2007;74(2):483–9.
[25] Yaraşir MN, Koca A, Kandaz M, Salih B. Voltammetry and spectroelectrochemical behavior of a novel octapropylporphyrazinato lead(II) complex. J Phys Chem 2007;111:16558–63.
[26] Donzello MP, Ou Z, Dini D, Meneghetti M, Ercolani C, Kadish KM. Tetra-2,3 pyrazinoporphyrazines with externally appended pyridine rings. 2. Metal complexes of tetrakis-2,3-[5,6-di(2-pyridyl)pyrazino]porphyrazine: linear and nonlinear optical properties and electrochemical behavior. Inorg Chem 2004;43(26):8637–48.
[27] Donzello MP, Dini D, D'Arcangelo G, Ercolani C, Zhan R, Ou Z, et al. Porphyrazines with annulated diazepine rings. 2. Alternative synthetic route to tetrakis-2,3-(5,7-diphenyl-1,4-diazepino)porphyrazines: new metal complexes, general physicochemical data, ultraviolet–visible linear and optical limiting behavior, and electrochemical and spectroelectrochemical properties. J Am Chem Soc 2003;125:14190–204.
[28] Marcos MT, Marcelo F, Catalani HL, Araki K, Henrique ET. Spectroelectrochemical and photophysical properties of a (3,4-pyridyl) porphyrazine supermolecule containing four $[Ru(bipy)_2Cl]^+$ groups. J Photochem Photobio A Chem 1998;118(1):11–7.
[29] Kissinger PT, Heineman WR. Laboratory techniques in electroanalytical chemistry. 2nd ed. New York: Marcel Dekker; 1996. pp. 51–163.
[30] Lever ABP, Milaeva ER, Speier G, Leznoff CC. The redox chemistry of metallophthalocyanines in solution. Phthalocyanines properties and applications, vol. 3. New York: VCH; 1993. pp. 5–27.
[31] Rollmann LD, Iwamoto RT. Electrochemistry, electron paramagnetic resonance, and visible spectra of cobalt, nickel, copper, and metal-free phthalocyanines in dimethyl sulfoxide. J Am Chem Soc 1968;90:1455–63.
[32] Donzello MP, Agostinetto R, Ivanova SS, Fujimori M, Suzuki Y, Yoshikawa HJ, et al. Tetrakis(thiadiazole)porphyrazines. 4. direct template synthesis, structure, general physicochemical behavior, and redox properties of Al (III), Ga (III), and In (III) complexes. Inorg Chem 2005;44:8539–51.
[33] Donzello MP, Zhongping O, Monacelli F, Ricciardi G, Rizzoli C, Ercolani C, et al. Tetra-2,3-pyrazinoporphyrazines with externally appended pyridine rings. 1. Tetrakis-2,3-[5,6-di(2-pyridyl)pyrazino]porphyrazine: a new macrocycle with remarkable electron-deficient properties. Inorg Chem 2004;43:8626–36.
[34] Donzello MP, Ercolani C, Stuzhin PA. Novel families of phthalocyanine-like macrocycles—porphyrazines with annulated strongly electron-withdrawing 1,2,5-thia/selenodiazole rings. Coord Chem Rev 2006;250:1530–61.